Fluid structure interaction between a pendulum and focused breaking waves

Bos, R. W.; Wellens, P. R.

DOI
10.1063/5.0054426

Publication date
2021

Document Version
Final published version

Published in
Physics of Fluids

Physics of Fluids

Fluid structure interaction between a pendulum and focused breaking waves

Cite as: Phys. Fluids **33**, 062118 (2021); https://doi.org/10.1063/5.0054426
Submitted: 18 April 2021 • Accepted: 02 June 2021 • Published Online: 29 June 2021

R. W. Bos and P. R. Wellens

Physics of Fluids ARTICLE scitation.org/journal/phf

Fluid structure interaction between a pendulum and focused breaking waves

Cite as: Phys. Fluids **33**, 062118 (2021); doi: 10.1063/5.0054426
Submitted: 18 April 2021 · Accepted: 2 June 2021 ·
Published Online: 29 June 2021

R. W. Bos and P. R. Wellens[a)]

AFFILIATIONS

Delft University of Technology, Mekelweg 2, Delft, The Netherlands

[a)]Author to whom correspondence should be addressed: P.R.Wellens@tudelft.nl

ABSTRACT

To study how an extreme wave load on a maritime structure causes structural deformation, an experiment is conducted to measure the response of a one degree-of-freedom pendulum in a focused, breaking wave. The tube that makes up the base of the pendulum covers almost the entire width of the tank so that three-dimensional effects can be considered small. The experiment varies the focus location with respect to the position of the pendulum as well as the vertical clearance between pendulum and mean free surface. Although the energy of the wave input was the same for all experiments, the response of the pendulum varied greatly with small variations of initial vertical clearance and wave focus location, with the wave breaking farthest away from the pendulum causing the largest response. A reduced-order model for the response of the pendulum shows the same behavior when initial clearance and focus location are varied. Even when initial clearance and focus location were kept the same between tests, large variability of the pendulum response was observed, meaning that the impulse exerted by the wave must have been different. This is different from the literature on breaking waves against rigid walls that found that local pressures show variability between experiments but that the impulse typically is the same. The experimental data and a description have been made available.

INTRODUCTION

Safe containment of liquefied natural gas (LNG) during transit requires hydroelastic evaluation of load and structural response. Predicting the time evolution of the structural deformation during a breaking wave impact by means of a numerical method is challenging. This article is about an experiment for a fundamental deforming structure in a breaking wave that may serve as a benchmark for numerical methods. The experimental data and a description thereof are available as open data (Wellens and Bos, 2021).

LNG will play a large role in making the maritime industry sustainable by replacing other more polluting fuels (Bureau Veritas, 2018). It is possible to safely transport LNG at -162° when the tanks are either nearly full or nearly empty. This avoids waves on liquid cargo, which are the waves that can significantly damage the structure. Because the temperature of LNG would make the ship brittle, the tanks are fitted with insulation, called a cargo containment system (CCS) (Issa *et al.*, 2009). When using LNG as fuel, the tanks will become less and less full, at some point creating the ideal situations for large breaking waves inside the tanks. Breaking waves pose a key challenge for the insulating membrane of LNG fuel tanks compared to the more traditional LNG cargo tanks.

Impacts of a breaking wave against a wall without hydroelasticity have been studied in detail: Lugni *et al.* (2006) considered the flip-through wave impact with detailed Particle Image Velocimetry (PIV) measurements and report vertical flow accelerations of 1500 g. Also for sloshing, it is noted that breaking waves give higher loads than waves that do not break (Ibrahim, 2020). Lugni *et al.* (2010) focused on the entrapped air cavity in a plunging breaking wave against the wall, whereas van Meerkerk *et al.* (2020) measured the free surface in the tip of the plunger to study instabilities that would lead to variability in the pressure during impact.

A typical way to decrease the variability is not to look at local pressures, but rather at the pressure impulse (Peregrine, 2003; Ghadirian and Bredmose, 2019). This is the time integral of a local pressure, thus integrating out the variability in time. Alternatively, the pressure can be integrated over the structure to obtain a force or moment, effectively reducing the variability in the spatial dimension. This is discussed in van de Bunt *et al.* (2021), with the main benefit that the force relates well to the modal response.

In Bogaert *et al.* (2010), sloshing is examined with more focus on the structure by sending breaking waves to a wall, modeling the insulation of an LNG tank of a ship. It is mentioned that a local impact load can lead to global deformation of the structure. For slamming, closely related to sloshing, hydroelasticity was investigated in, for instance, Faltinsen (1997) and Wang *et al.* (2019). Two impact phases are distinguished here: the structural inertia phase in which the beam accelerates due to an impact, and the free vibration phase in which the structure is submerged. Experimental validation shows that this distinction is valid. Lugni *et al.* (2014) considered the hydroelastic slamming response in shallow-liquid sloshing with a hybrid experimental/numerical method with overall good results. The maximum peak pressure was only found to correspond to the experiment when the added mass effect was considered. The hybrid method was, however, not able to reproduce the time evolution of the deformation of the structure.

Breaking wave impacts are not limited to situations with sloshing. Cheng and Ji (2020) studied breaking wave impacts on a wind turbine foundation pile with nonlinear potential flow and a high-order boundary element method. Another closely related problem is wave impacts for green water which are, for instance, investigated in Cox and Ortega (2002) and Ariyarathne *et al.* (2012). A lab experiment is conducted to study a transient wave impact on a deck above the free surface. Similar impact loads of plunging breaker on a tension-leg platform (TLP) in 2D are discussed in Chuang *et al.* (2017), where the void fraction of the water hitting the structure is taken into account. Taking the void fraction into account gave a more accurate estimate of the impact coefficients, which predict the maximum impact pressure. Additionally, one could take the pressure impulse, which is more repeatable than the maximum pressure (Peregrine, 2003). However, for the structural response, the exact temporal and spatial distribution of the load matter, especially when considering that the load also depended on the motion of the structure.

As mentioned in Bos and Wellens (2021), fluid structure interaction for maritime applications (or hydroelasticity) has the following properties. It has high added mass and large changes in wetted area, and the structures are heavy and stiff in local deformation. Hydroelasticity is considered especially important in extreme events such as slamming, sloshing, and green water. Impacts on freely floating maritime structures during these events are a combination of many processes (Lafeber *et al.*, 2012), but they consist mainly of four phases (Bos and Wellens, 2021):

1. The wetted area of the structure increases/impact problem.
2. The structure is fully submerged and vibrates with a maximum of added mass and damping.
3. Wetted area decreases as the structure emerges from underwater.
4. Free vibration of the structure with all energy that has been transferred.

The behavior during the first phase depends on the shape of the incoming wave, as outlined in Lafeber *et al.* (2012) and Peregrine (2003). Another important challenge is to account for the variability inherently present in wave impacts (Frihat *et al.*, 2016).

All four phases of fluid–structure interaction are important and, accordingly, validation problems including all these phases are required. With the experimental setup described in this article, we aimed to devise the simplest possible experimental model of a maritime structure that is free to move in extreme conditions, in order to study the variability of wave impacts. The maritime structure is modeled as a pendulum suspended above the mean free surface a towing tank. Focused waves are generated to simulate an extreme event in a sea state. The focused wave breaks near the structure and makes the structure undergo all four wave impact phases.

Traditionally many of these experiments have been performed with a rigid or flexible wall as a structure, such as the sloshing experiments described by Bogaert (2018) and Ibrahim (2020). Mai *et al.* (2020) considered drop tests and wave impact tests with hydroelasticity. It showed that high aeration reduces the impact force for the flip-through and slightly breaking wave. The total force impulse decreases for the elastic wall, whereas the total pressure impulse increases. Hence, the scale of structure that is considered matters for whether hydroelasticity is important.

An advantage of the pendulum over a wall is that the maximum pendulum response is a measure of the impulse, force integrated over time, on the structure placed at a relevant position. The relevant position in our case is near to where the wave breaks since that is where the highest forces are expected. An additional advantage is that the experimental setup with the pendulum above the mean free surface allows for a meaningful, almost undisturbed measurement of the wave near the pendulum, so that input to and response of the pendulum system can be compared in order to study the variability. This setup is inspired by Mathai *et al.* (2019), who achieved good modeling accuracy for a submerged pendulum.

THE EXPERIMENT AND THE REDUCED-ORDER MODEL

With this experiment, we want to increase the fundamental understanding about fluid–structure interaction in extreme wave events for maritime applications as well as provide reproducible validation data. This experiment uses a similar setup to Bos and Wellens (2021); the setup is explained first. An important addition to the original setup is the focused wave, so the second section describes how the waves are designed and generated. After that a reduced-order model is presented with which the experiment is compared.

Experimental setup

Figure 1 shows a side view of the small towing tank at Delft University of Technology. The structure that we call pendulum has rotation around a fulcrum as its only degree of freedom. It is shown in the middle of Fig. 1, suspended from the towing carriage and close to being impacted by the wave. On the far left is the wave absorbing beach and on the far right the flap type wave maker. Three wave gauges are mounted before, at, and after the pendulum to measure the surface elevation before during and after interaction with the pendulum. The rotation of the pendulum is measured with a potentiometer, which goes to the same measuring system as the wave gauges. An analog second order filter with a cutoff frequency of 100 Hz is used, and the data are sampled at 1000 Hz. A 250 fps camera records the motion of the pendulum and the evolution of the wave profile from the side, which is later synchronized with the measuring system using the frame in which the pendulum starts to move.

A photo of the pendulum is shown in Fig. 2 and consists of a frame and a horizontal tube. The frame is made of stiff aluminum profiles, with two strips extending from the bottom of the frame, holding the polyvinyl chloride (PVC) tube with a diameter of 50 mm. The tube, almost as long as the towing tank, is wide so that three-dimensional

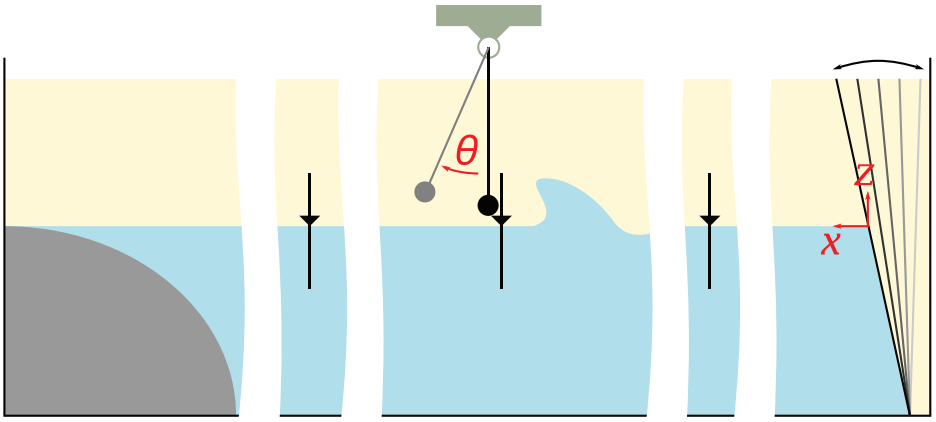

FIG. 1. Schematic overview of the experimental setup. At the far left side, the beach, and at the far right, the wave maker with the axis system. In between, the three wave gauges at 25.849, 29.880, and 34.666 m from the wave maker as well as the pendulum at 29.880 m from the wave maker.

effects can be considered small. The main thought behind this configuration is that only the tube has hydrodynamic interaction with the wave and that, because of its circular cross section, the hydrodynamic interaction does not depend on the rotation of the pendulum. The hydrodynamic interaction with the strips between frame and tube can be neglected. The length of the pendulum from the center of the tube to the fulcrum measures 1050 mm. We know from a least squares fit of free vibration experiments in Bos and Wellens (2021) that the structural properties of the pendulum are $I = 2.17\,\mathrm{kg\,m^2}$, $c = 0.205$ N m s rad^{-1}, and $k = 31.7$ N m rad^{-1}, with I the inertia, c the damping, and k the restoring coefficient. The water depth is constant throughout the experiment at 995 mm.

The wave gauges were calibrated and the maximum difference between measured points and the linear fit was less than 0.5 mm over its entire range; for the potentiometer, the maximum difference was less than 0.5°. The camera was focused and calibrated on the window in the side of the tank at the pendulum location. The recorded images have a resolution of 0.3 mm/px.

The tests in the experiment varied the focus location of the wave components (see "Wave generation" section) and the clearance between the mean water level and the bottom of tube. Each test was repeated five times. All tests with the same configuration were performed after each other, with a waiting time in between tests of at least 15 min. This allowed the water to come to rest, with "rest" defined by the situation that the remaining free surface oscillations were lower than the calibration error of the wave gauge.

Wave generation

A breaking wave was generated at different locations in the tank by focusing wave components toward four focus locations in the tank at positions $x_{foc} = 29.880, 29.380, 28.880, 28.380$ m with respect to the wave board. The latter focus position is the location of the pendulum itself. Relative to the pendulum, the focus points are defined as $f = 0.0, -0.5, -1.0, -1.5$ m (in reverse order). Wave breaking takes time and distance to develop. The wave that focuses at the position of the pendulum, breaks somewhat further down the tank. It is therefore an example of unbroken wave interaction with the pendulum. The wave that focuses half a meter before the position of the pendulum gives interaction with the steep, undisturbed front of the breaking wave. The waves that break at 1 and 1.5 m before the position of the pendulum have already overturned when reaching the pendulum and are therefore examples of aerated wave interaction with the pendulum.

Figure 3 shows three of the ten components that we used to generate the breaking waves, with a windowing function that ramps the signal up and down so that discrete wave groups or are created. In this way, wave breaking near the wave board is prevented, which reduces the variability of the unbroken free surface signal at wave gauge 1. The wave lengths (or, equivalently, periods) of the components were selected in such a way that ramp-down of a shorter component overlaps with the ramp-up of a longer component. The wave lengths of the components in ascending order are $\lambda_i = (1.00, 1.10, 1.25, 1.45, 1.70, 2.00, 2.40, 2.90, 3.60, 5.00)$ m. The amplitudes of the wave

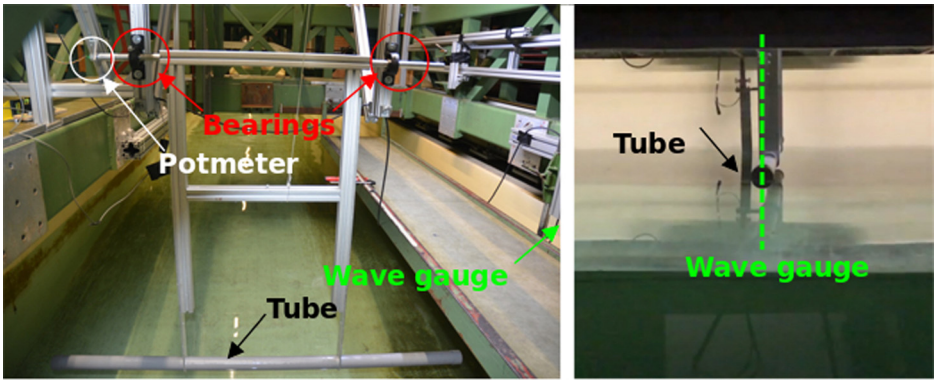

FIG. 2. Photos from front (left) and side (right) of the experimental setup, showing the tube, the frame, bearings, potentiometer, and wave gauge nearest to the pendulum.

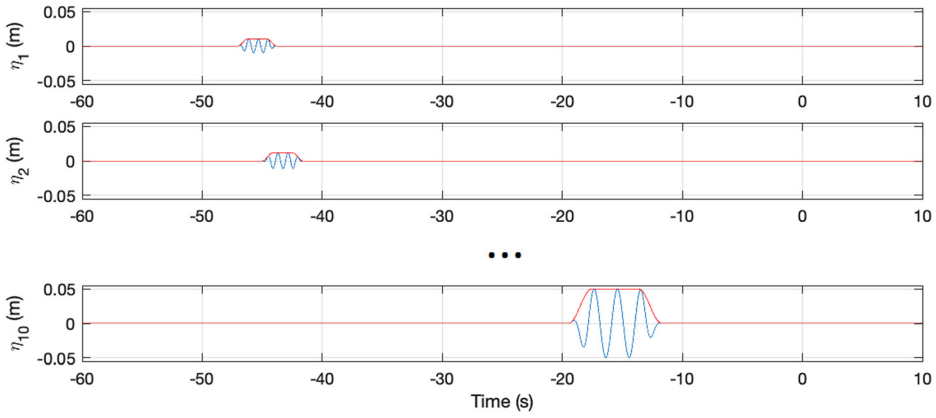

FIG. 3. Surface elevation over time at the position of the wave board. The first, second, and final wave components of the focused wave (with window function to create groups).

components were found by giving each wave component a maximum steepness $H_i/\lambda_i = 1/50$, with H_i the wave height of the component. For this steepness the wave propagation of an individual component can reliably be predicted with linear theory. Wave components with lengths lower than 1.00 m or with a steepness higher than 1/50 give significant variability (with the wave maker in our tank), and wave lengths longer than 5 m with this steepness were limited in amplitude by the maximum stroke of the wave board.

The window function has two benefits and one downside, in addition to the fact that it prevents wave breaking near the wave board. First, it limits the stroke of the wave maker as not all components have to be generated at the same time. Second, it minimizes early nonlinear interactions because the wave groups themselves have a small steepness and only add up and interact near the pendulum. It means little difference between the linear group and phase velocity and what is obtained in the tank. Practically, this means that the location of focus location can be reliably predicted. The downside of windowing is however that the ramp up and down introduces additional, mostly shorter, wave components, causing the wave group to lose energy along the way. Altogether, this means that although location of where the wave components converge is well predicted, but that the obtained surface elevation is lower than the sum of the amplitudes of the wave components. For the wave focused at $f = 0.0$ m, we can confirm that the measured maximum surface elevation is lower than the expected maximum.

The window function can be described as follows. It ramps up the surface elevation of a component from 0 to the desired maximum surface elevation over a single wave period by means of a negative cosine function with twice the period and a shifted mean. Then the window function equals 1 for the duration of two wave component periods before ramping the surface elevation down again over one wave component period. The phase shift of a component is chosen such that the middle full-height peak of this four-period window for each wave component arrives at the focus location f at time $t = 0$. Then the window functions are moved back in time with the group velocity over the distance between the pendulum and wave maker to know when the wave maker should start generating these components with the appropriate phase and amplitude.

Reduced-order model

In addition to the experiment, a reduced-order model is employed to predict the response. The reduced-order model can be used to determine what the dominant force components are in the interaction between breaking wave and pendulum. In Bos and Wellens (2021), the reduced-order model is found to compare well to experimental results for interaction of the pendulum monochromatic waves. Here, we use the same model for the interaction with breaking waves, with the same structural coefficients and the same hydrodynamics coefficients as in the setup with monochromatic waves.

The reduced-order model is based on the equation of motion of the pendulum,

$$I\ddot{\theta} + c\dot{\theta} + k\sin\theta = M, \tag{1}$$

with pendulum angle θ, moment of inertia I, damping coefficient c, and stiffness k. The external moment due to wave loading is denoted by M. M is defined as

$$M = \beta F_m L\cos\theta, \tag{2}$$

with L the distance between the fulcrum and the center of the tube, and F_m the Morison force (Morison *et al.*, 1950),

$$F_m = \rho\left(C_m V a + \frac{1}{2}C_d A|u|u\right), \tag{3}$$

containing the density of the water ρ, submerged volume V, frontal area A, and the relative velocity u and relative acceleration a. The coefficients for added mass $C_m = 1.0$ and drag $C_d = 2.0$ are similar to Sarpkaya (1986). This leaves only β to be defined: it is the wetness parameter of the tube, introduced by Bos and Wellens (2021), denoting how far the pendulum is submerged,

$$\beta = \max\left(\min\left(\frac{\eta - (z_p - D/2)}{D}, 1\right), 0\right), \tag{4}$$

with D the tube diameter, η the wave elevation, and z_p the instantaneous vertical position of the center of the tube with respect to the mean free surface, defined as $z = 0$. This model is integrated over time using a Runge–Kutta two scheme with $dt = 0.05$ s, which gives a numerical error smaller than the calibration error of the potentiometer, even after seven full periods of free vibration (Bos and Wellens, 2021).

The Morison equation with the wetness parameter requires the fluid height, fluid velocity, and fluid acceleration at the instantaneous position of the tube center. The surface elevation signal measured at

wave gauge 2 is transformed to its Fourier components, with a complex amplitude. The amplitudes and phases are used in linear potential wave components (Airy wave components) to determine the velocity and acceleration amplitude vectors per component at the instantaneous position of the center of the tube, after which the complex velocity and acceleration amplitude vectors are transformed back to time signals. Note that constant extrapolation is used for the velocities and acceleration above the mean free surface at $z = 0$. We consider this a linearization of the fluid potential around the position of wave gauge 2 because linear potential wave theory is used to extrapolate the fluid velocities and accelerations to the instantaneous horizontal and vertical position of the tube center.

RESULTS AND DISCUSSION

In the experiment, the focus location of the wave components and the clearance of the bottom of the pendulum with respect to the mean free surface is varied. The amplitudes of the wave components are not varied between tests; the wave system therefore always has the same energy content. The response of the pendulum is measured in degrees of rotation as a function of time and the maximum deflection can serve as a measure of the impulse exerted by the breaking wave on pendulum.

According to Peregrine (2003), breaking waves can have a higher front velocity compared to nonbreaking waves, leading to a higher maximum force. The presence of entrained air, on the other hand, can have a cushioning effect that reduces the force peak. It takes time and distance for a focused wave to overturn. Varying the distance between the focus location and the location of the pendulum, therefore, varies the interaction between the pendulum and the breaking wave in different stages of development. The focus location at the position of the pendulum will lead to unbroken wave interaction with the pendulum and no air entrainment, whereas the focus location farthest away from the pendulum will lead to interaction with a broken wave having entrained air.

The fluid velocities are largest near the crest of the breaking wave. Therefore, raising the pendulum by increasing the clearance between the bottom of the pendulum and the mean free surface exposes the pendulum to higher fluid velocities, with a larger maximum force. On the other hand, the wave is also narrower near the crest than below, so that the time over which the pendulum is exposed to the wave is shorter.

The following shows how changing the focus location changes the free surface elevation at the location of the pendulum and how that affects its response over time and its maximum response. It also shows how changing the clearance changes the response. We will discuss seven different configurations of focus location and clearance; for each configuration, five repetitions were performed to investigate the variability. A configuration is addressed by the test number of its first test.

Qualitative analysis

Figure 4 shows a snapshot of a wave impact for each configuration taken with the high-speed camera from the side, just before the pendulum starts to move. The pendulum's interaction with the wave in the different configurations is described below. The focus location f in the description is given in meter with respect to the position of the pendulum (negative means opposite to the direction of wave propagation). The clearance c is given in meter with respect to the mean free surface (more positive means further away from the free surface). In order of increasing distance between pendulum and focus location:

- series 500, $c = 0.05, f = 0.0$: steep wave, no breaking;
- series 505, $c = 0.05, f = -0.5$: steep wave, onset of breaking, pendulum low;
- series 605, $c = 0.10, f = -0.5$: steep wave, onset of breaking, pendulum near crest;
- series 510, $c = 0.05, f = -1.0$: overturning has started, pendulum low;
- series 600, $c = 0.10, f = -1.0$: overturning has started, pendulum near crest;
- series 515, $c = 0.05, f = -1.5$: overturning with jet re-entry and mixing, air entrainment, pendulum below aerated zone;
- series 600, $c = 0.10, f = -1.5$: overturning with jet re-entry and mixing, air entrainment, pendulum in aerated zone.

The wave interaction with the pendulum is analyzed later in terms of the front velocity upon impact, the front angle or orientation of the free surface upon impact, and the wave height. The amount of air present in the water upon impact is not quantified.

Free surface at the position of the pendulum

In Fig. 5, we see the free surface at the position of pendulum, measured with the second wave gauge WHM2, for all configurations. The time signal of the focused wave components at the focus location is designed to be symmetrical with respect to the maximum free surface elevation, with lower waves on either side. The realization in the tank still features most of that design. Note that the focus location only coincides with the position of the pendulum for configuration 500. For the other six configurations, the wave gauge is farther away from the wave board than the focus location. The first two wave crests in the time signals pass underneath the pendulum without touching it. The third crest makes an impact with the tube of the pendulum, after which the remaining crests pass underneath without engaging with the pendulum anymore. There is one impact event per test.

In anticipation of the reduced-order model results, Fig. 5 also shows the Fourier reconstruction of the signal when truncated to 40 Hz. Wave components above that frequency would have a wavelength of 1 mm, which is thought to be beyond the measurement accuracy of the setup. The reconstructed signal is identical to the measured signal except for an almost imperceivable difference (1 mm) near the peak.

Compared to Fig. 5, Fig. 6 gives a more detailed representation near the peak of the free surface as a function of time, together with the free surface measurements from processing the last 25 camera images before the pendulum starts to move. The processing involved a Sobol filter to highlight edges in the images, the free surface being the brightest edge, after which a seventh order polynomial was fitted through the free surface. The differences in free surface between different realizations of a configuration were generally small. The free surface from the images also compares well to the signal from the wave gauge, but not for configuration 520. Here, the five different realizations give different results that are also dissimilar from the wave gauge signal. Upon careful inspection, we find that also the wave gauge signals for the five realizations of configuration 520 are dissimilar from

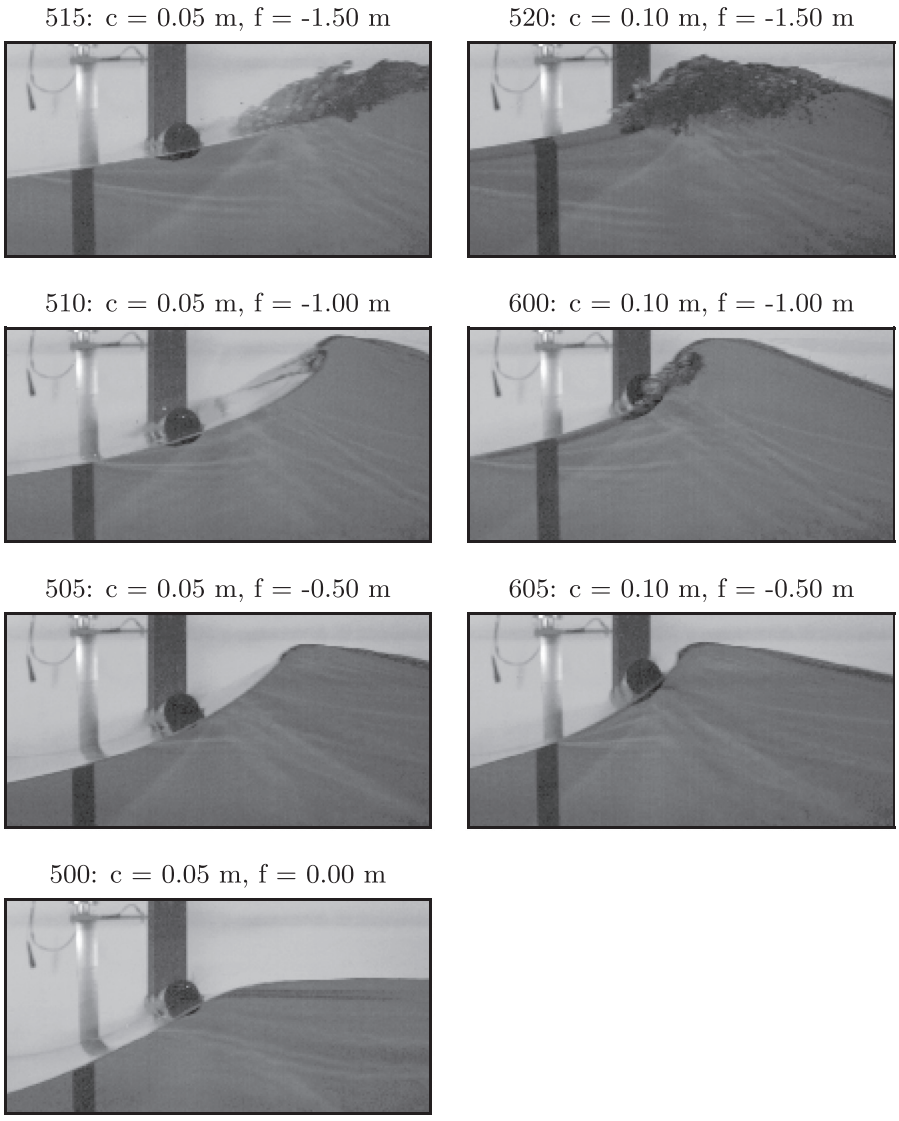

FIG. 4. Snapshot of free surface just before the pendulum starts to move with *c* as clearance between the bottom of the pendulum and the mean free surface and *f* as focus distance with respect to the pendulum (negative is toward wave maker).

each other near the peak. Series 510 and 520 feature waves with a lot of mixing compared to the other series and with air entrainment. We now have to ask the somewhat philosophical question of what "free surface" means in a measurement with a resistive wave gauge in a water–air mixture. The free surface in the images appears to be less ambiguous: it is simply the dividing line between what can be considered air on the one side, and every mixture of water and air on the other. In any case it is clear that the realizations of waves with developed mixing regions and a high air content, such as for configuration 520, are different from each other, much more than before re-entry and mixing.

Figure 7 shows the free surface as a function of position at the time instant just before the pendulum started to move. The free surface is reconstructed from the image for that time, and also for 20 and 40 ms before that time to show the evolution of the free surface. The elevation measured by the wave gauge is also indicated at the position of the wave gauge for the time of impact. There is agreement between the free surface from the images and the wave gauge for all configuration, except for configuration 520. Here the wave gauge measurement of the free surface for the water–air mixture is different from what is detected in the images. Note that the different realizations for configuration 520 in space are not that dissimilar from each other. The differences only become larger in the last 5 cm before the position of the pendulum.

Figure 7 also shows the reconstruction of the free surface as a function of position that is obtained from the complex amplitudes of the Fourier transform of the time signal of wave gauge 2, together with the wave numbers resulting from the linear dispersion relation. The reconstruction gives a reasonable impression of the wave shape, but is clearly not a good quantitative estimate of the position of the free

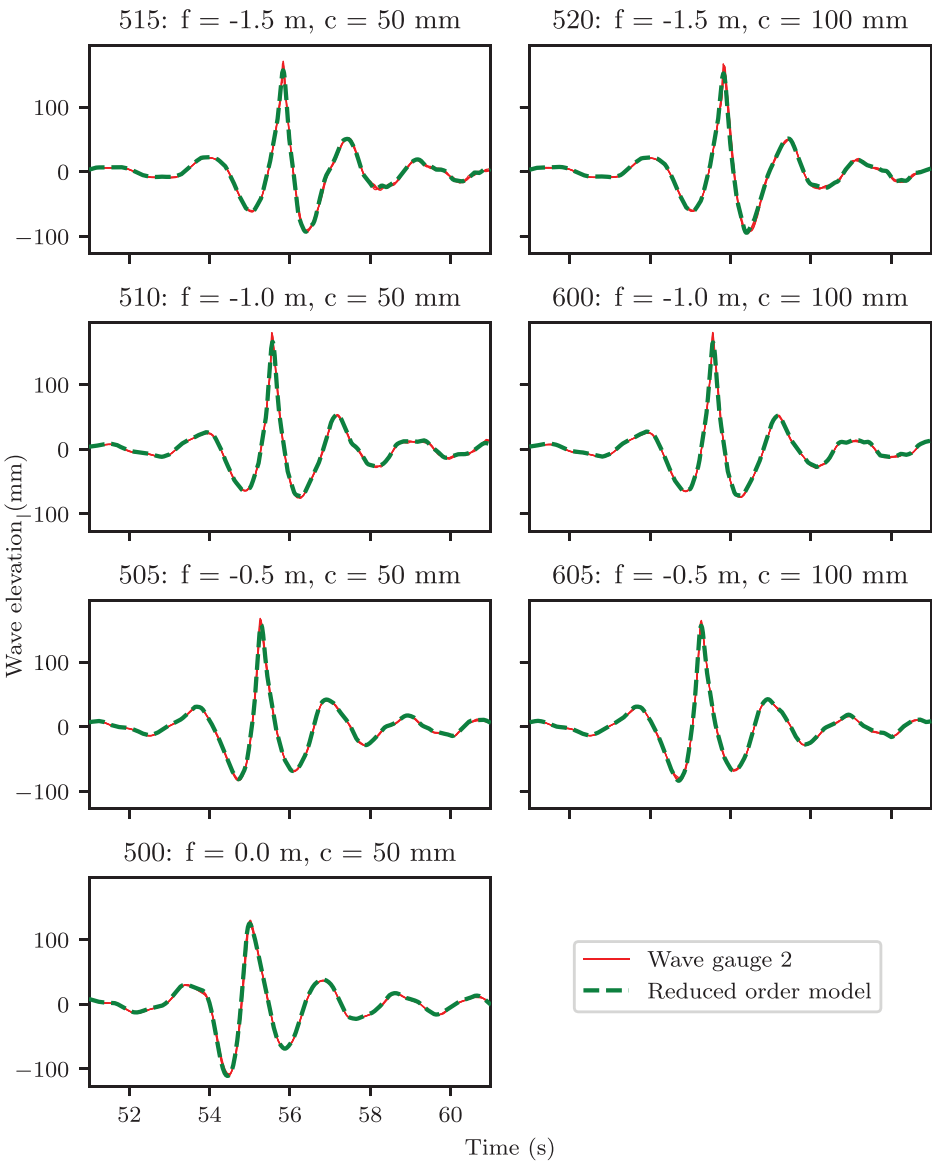

FIG. 5. Surface elevation over time at the position of the pendulum (wave gauge 2); the reconstructed signal intended as input for the reduced-order model is compared to the experiment.

surface because linear wave theory is used far beyond the range of validity of the expansion around the mean free surface and because many of the wave components in the Fourier transform are bound, nonlinear components, and not free, propagating components. This already gives some account of the expected accuracy of the reduced-order model.

Maximum pendulum response

Figure 8 provides a summary of all interaction events between the pendulum and the breaking waves. The vertical axis shows the maximum response angle θ of the pendulum, which is a measure of the impulse exerted on the pendulum. Three horizontal axes show the front velocity upon impact v, the front angle upon impact α, and the maximum surface elevation η measured at wave gauge 1 and 2. The front velocity and the front angle are determined from the camera images. The moment of impact is determined as the time instant of the image just before the pendulum starts to move. There were some difficulties determining the front velocity and front angle in configuration 520 in which a lot of air is present just below the interface. In these cases, the last unambiguous measurement was used, which was 20 ms before impact in one case and 40 ms before impact in another.

The tests with configurations 515 and 520, involving the mixing and the air entrainment, gave the largest pendulum response. They also show the largest spread in the pendulum response. The pendulum response for the other configurations is more clustered. From series 515, it appears as if the largest front velocity correlates with the largest pendulum response. From series 510 on the other hand, it appears as

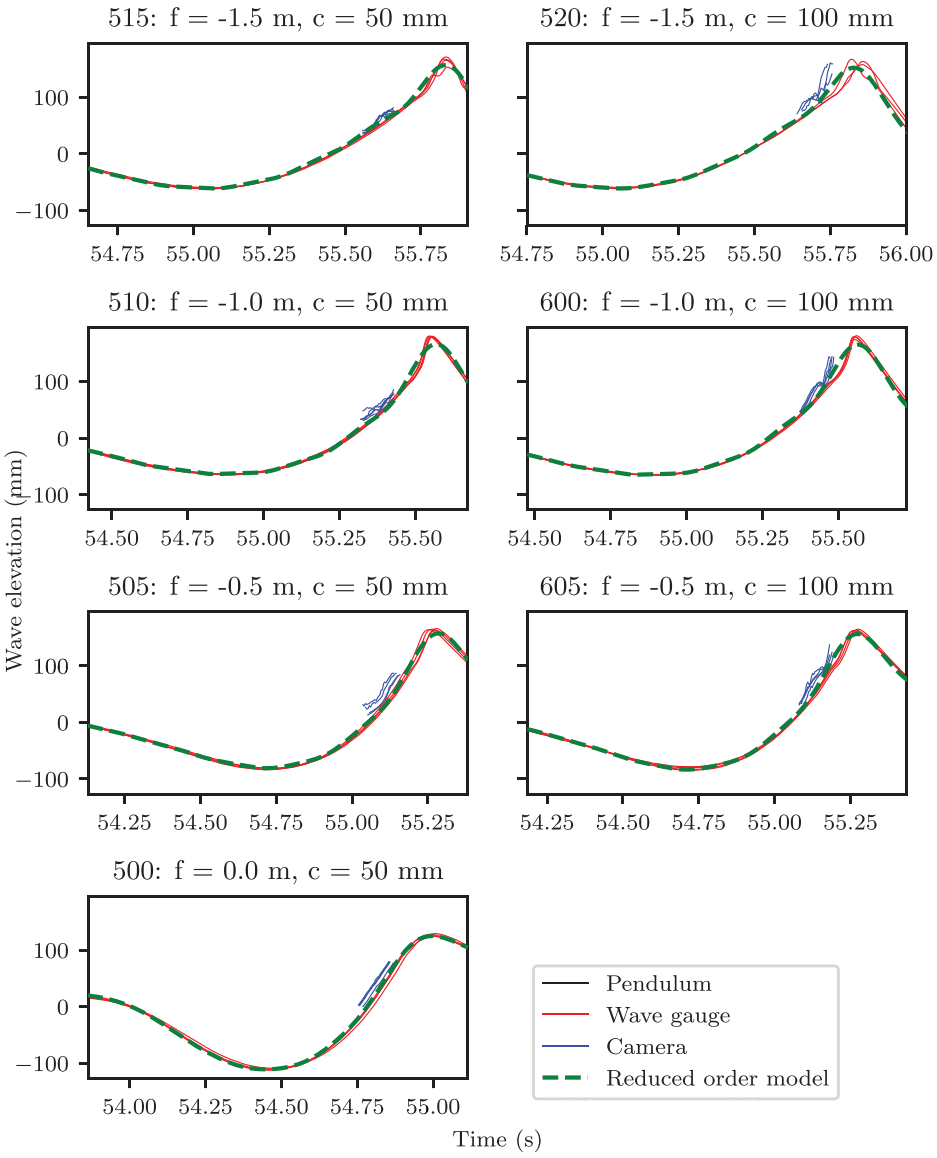

FIG. 6. Surface elevation over time at the pendulum close to the moment of impact with the breaking wave; measurements of wave gauge 2 are compared to the surface elevation detected in the camera images.

if the maximum pendulum response has no relation with the front velocity at all. From series 520 it appears as if the largest front angles (steepest wave front) correlate with the largest pendulum response, but from series 515 it seems that the larger pendulum response correlates with a lower front angle. The largest surface elevation measured at wave gauge 2 (at the position of the pendulum) does not coincide with the largest pendulum angle, and from series 500, we find that a surface elevation that was on the low side of what was measured can lead to a larger pendulum response than the highest surface elevations measured for series 600. Unlike all other configuration, series 500 with the unbroken wave, has a straightforward relation with the maximum pendulum response: the variability of the surface elevation is immediately transferred to a variability of the pendulum response. The variability at wave gauge 2 is due to the wave components converging near the pendulum and the subsequent nonlinear exchange of energy between components because hardly any variability in the surface elevation is present at wave gauge 1. The variability for series 515 and 520 is most likely due to mixing and air entrainment.

Table I presents an overview of the average value of the main parameters, together with its coefficient of variation (cov, standard deviation over average value). The average value of the maximum pendulum response is largest for configuration 600, with the developed mixing zone and the air entrainment. The cov of the maximum pendulum response is larger for both configurations with the mixing zones and the air content than for the other configurations. Table I does not reveal a clear trend for the average value of maximum pendulum response vs the average values of any of the other parameters. There is a clear trend for the cov: when the cov of the surface elevation is larger, also the cov of the maximum pendulum response is larger. When the cov of the surface elevation is lower, also the cov of the

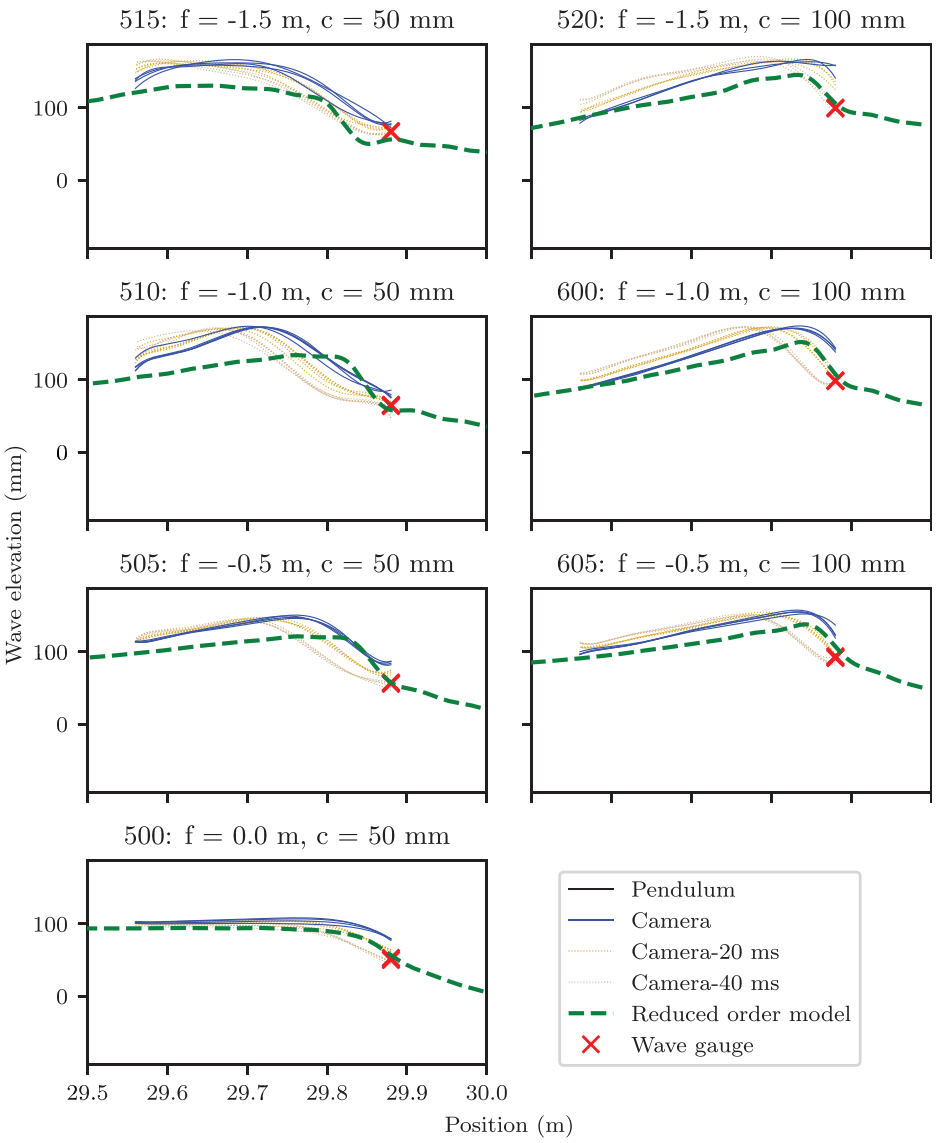

FIG. 7. Surface elevation as a function of position close to moment of impact with the breaking wave; free surface reconstruction intended for the model is compared to the free surface from the camera image before pendulum motion is detected.

maximum pendulum response is lower. The cov of the maximum pendulum response is always larger than the cov of the maximum surface elevation. Similar trends for the coefficients of variation of the other parameters could not be identified. It is special for this system with a degree-of-freedom that there is variability of the global response at all and, hence, of the impulse. Studies with similar breaking waves and rigid walls have shown that although differences in local pressures were measured between repetitions, the total impulse was approximately constant (Hofland *et al.*, 2010; Bullock *et al.*, 2007).

We expected a stronger correlation between the maximum pendulum response on the one hand, and the three parameters front velocity, front angle and surface elevation on the other. An explanation for the absence of such a correlation with the front velocity and the front angle can be that the impact force, although large, has a short duration compared to time that the tube of the pendulum is submerged. The absence of a correlation between the average maximum surface elevation and the average maximum pendulum response cannot be explained in this way because of the following effects. A higher wave has higher fluid velocities that will lead to a higher drag force, and on many occasions, the increased surface elevation also means that the pendulum is submerged and exposed to drag for a longer time. These effects are considered in more detail in the "Reduced-order model results" section where the results of the reduced-order model are presented.

Reduced-order model results

From the summary of the experimental results, it was found that wave front velocity and front angle do not show a strong correlation with the maximum pendulum response. A reduced-order model was

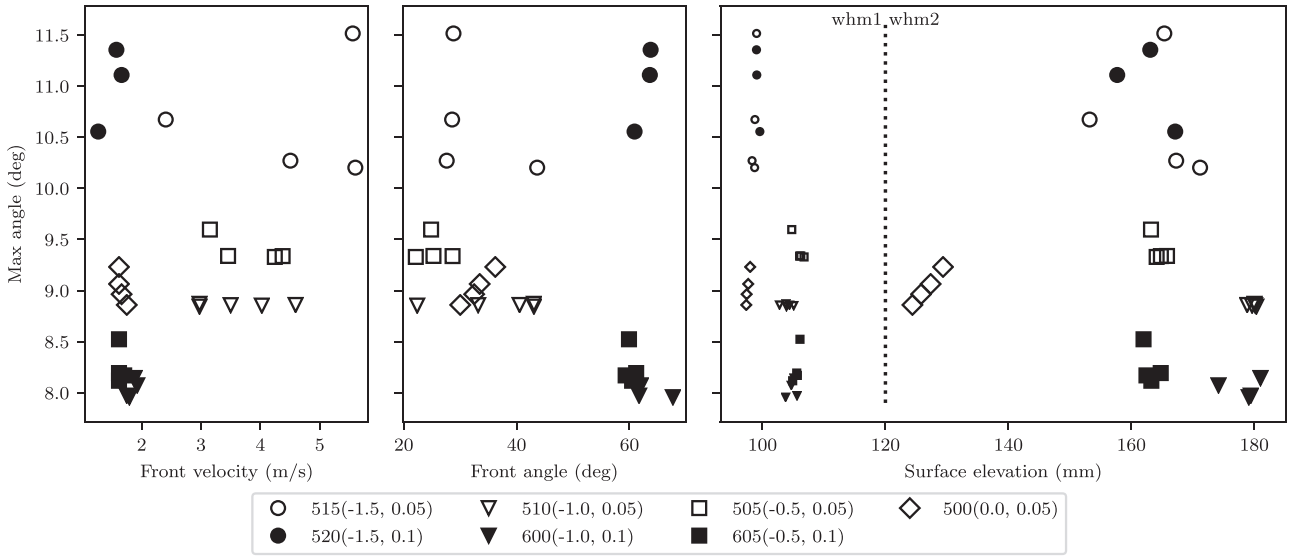

FIG. 8. Maximum pendulum response vs (from left to right) maximum front velocity v, front angle α and surface elevation η at wave gauge 1 and 2.

presented above that does not include the wave impact force, but does include the transition from dry to wet, the submerged exchange of momentum, and the transition from wet to dry. Note that the surface elevation signal of wave gauge 2 at the position of the pendulum was transformed to linear Fourier components and that the complex amplitude of these components was used to reconstruct a fluid velocity and fluid acceleration at the instantaneous position of the center of the tube by means of linear Airy theory. Velocity and acceleration are input to computing the force with the Morison equation. Figure 9 shows the different components of the computed force for the different configurations. It is immediately clear that the total force on the pendulum is dominated by drag. For the same breaking waves (focus location the same), the maximum absolute force on the tube is higher when the clearance is smaller. The duration of the force is also longer when the clearance is smaller. Considering especially the left column of Fig. 9, for the smaller clearances, we may now also have an explanation why there is no direct correlation between the maximum surface elevation and the maximum pendulum response. The motion of the pendulum is counteracted by a force in the other direction. When the maximum surface elevation becomes larger, also the counteracting force becomes larger and longer in duration.

Figure 10 compares the results of the reduced-order model for the pendulum response as a function of time with the pendulum response that was measured in the experiment. The time signal shows the pendulum being exposed to the breaking wave, followed by a free vibration. The difference between the reduced-order model result and the experiment is particularly small for configuration 500, with the nonbreaking interaction with the pendulum. Although the wave front for configuration 500 in Fig. 4 is rather steep, the reduced-order model with a local linearization of the flow field is a good approximation of the experiment with a difference near the maximum response of less than 1%. For configurations 505 and 605, the breaking wave is at the onset of overturning. The reduced-order model overestimates the response compared to the experiment with a difference of less than 10% for both configurations. It is interesting that the difference with the experiment is the same for 505 and 605, because the distance between the mean free surface and the center of the tube is larger for 605. Before seeing the results, we thought that the constant

TABLE I. Summary of the test results, ordered by focus location f and clearance c. Average (avg) and coefficient of variation (cov, standard deviation over average) is presented for maximum pendulum angle θ (°), maximum wave elevation η (mm) at wave gauge 2, front speed v (m/s) and front angle α (°).

Series (f, c)	avg θ	cov θ	avg η	cov η	avg v	cov v	avg α	cov α
515 (−1.5, 0.05)	10.7	5.66×10^{-2}	1.64×10^{2}	4.72×10^{-2}	4.52	3.31×10^{-1}	3.22×10^{1}	2.39×10^{-1}
520 (−1.5, 0.1)	11.0	3.72×10^{-2}	1.63×10^{2}	2.91×10^{-2}	1.50	1.38×10^{-1}	6.28×10^{1}	2.56×10^{-2}
510 (−1.0, 0.05)	8.86	1.11×10^{-3}	1.80×10^{2}	3.27×10^{-3}	3.61	1.94×10^{-1}	3.64×10^{1}	2.43×10^{-1}
600 (−1.0, 0.1)	8.04	1.10×10^{-2}	1.78×10^{2}	1.66×10^{-2}	1.84	4.35×10^{-2}	6.30×10^{1}	5.15×10^{-2}
505 (−0.5, 0.05)	9.40	1.39×10^{-2}	1.64×10^{2}	6.69×10^{-3}	3.81	1.57×10^{-1}	2.52×10^{1}	1.06×10^{-1}
605 (−0.5, 0.1)	8.25	2.23×10^{-2}	1.63×10^{2}	7.51×10^{-3}	1.64	2.67×10^{-2}	6.02×10^{1}	1.32×10^{-2}
500 (0.0, 0.05)	9.03	1.75×10^{-2}	1.27×10^{2}	1.69×10^{-2}	1.66	3.72×10^{-2}	3.30×10^{1}	7.78×10^{-2}

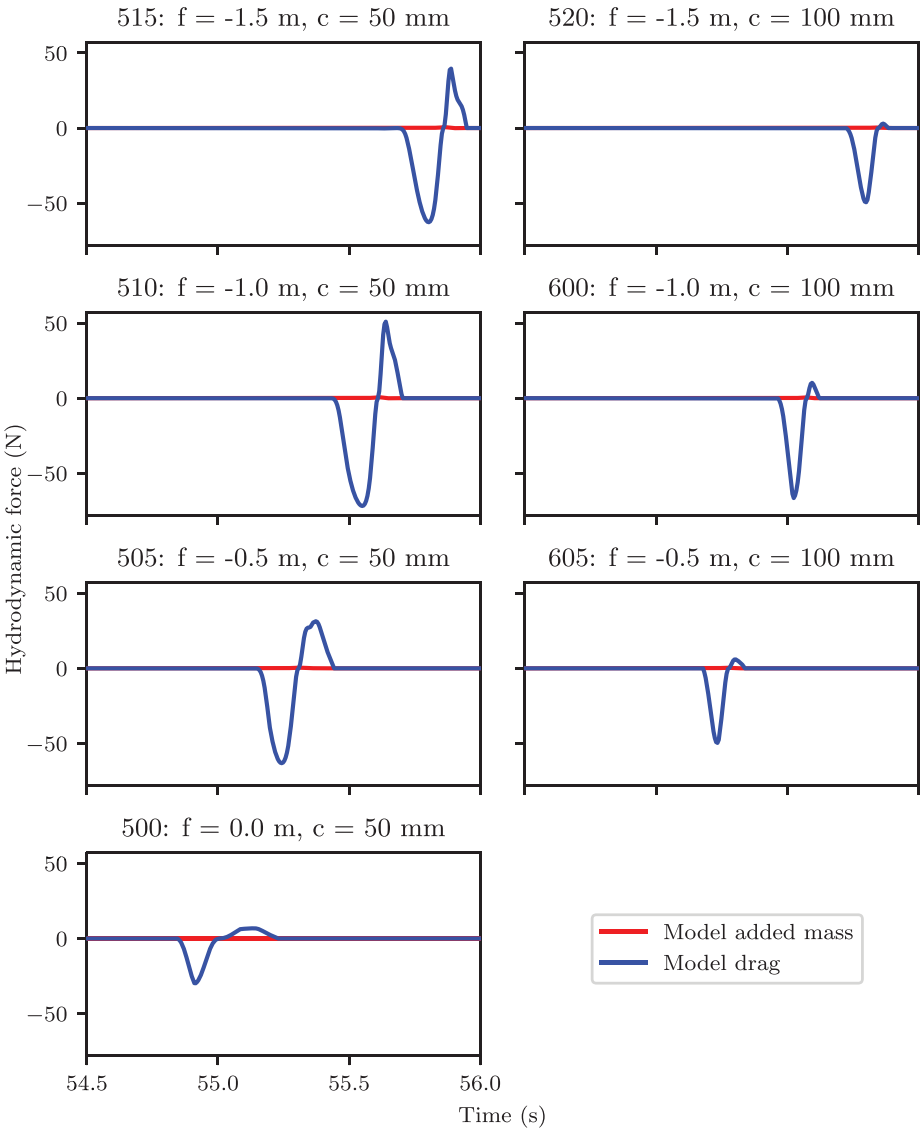

FIG. 9. Reduced-order model approximation of the force on the pendulum in a breaking wave for the different configurations of focus location and tube clearance (negative force is in the direction of wave propagation).

extrapolation of velocities above the mean free surface in the model would turn out worse for 605 than for 505, but it does not. The breaking wave has started overturning for configuration 510 and 600. In these configurations, the difference between the reduced-order model and the experiment is largest and too large to be called a good approximation. It is, however, a conservative estimation of the pendulum response. The reduced-order model for 510 overestimates the maximum response of the pendulum by 12%. For 600, the overestimation of the pendulum is response is close to 20%. Here, we do see that the difference between model and experiment increases when the clearance is increased, which could be the results of using constant extrapolation of the velocities and accelerations above the mean free surface.

What is unexpected is that the reduced-order model overestimates the maximum response; beforehand we would have estimated that the fluid velocities in a steep nonlinear breaking wave would be larger than those obtained from a linear approximation of the flow field in such a wave. The experiments for configurations 515 and 520, finally, have the most complex flow field with a developed mixing zone and some air content. The reduced-order model has less than 3% difference in the maximum pendulum response for 515 and 5% difference for 520, where for the other configurations the reduced-order model overestimates the maximum pendulum response. It gives an underestimation of the maximum response for 520. From Fig. 8, it was found that the mixing zone and the air content caused a comparatively large variability of the maximum pendulum response, but for 515 and 520, the reduced-order model is a good approximation of the experimental results on average. Overall, the reduced-order model gives a good account of the changes in maximum pendulum response for the different phases of wave breaking that we enforced by changing the focus location of the wave components and for the different elevations of the tube of the pendulum with respect to the mean free surface.

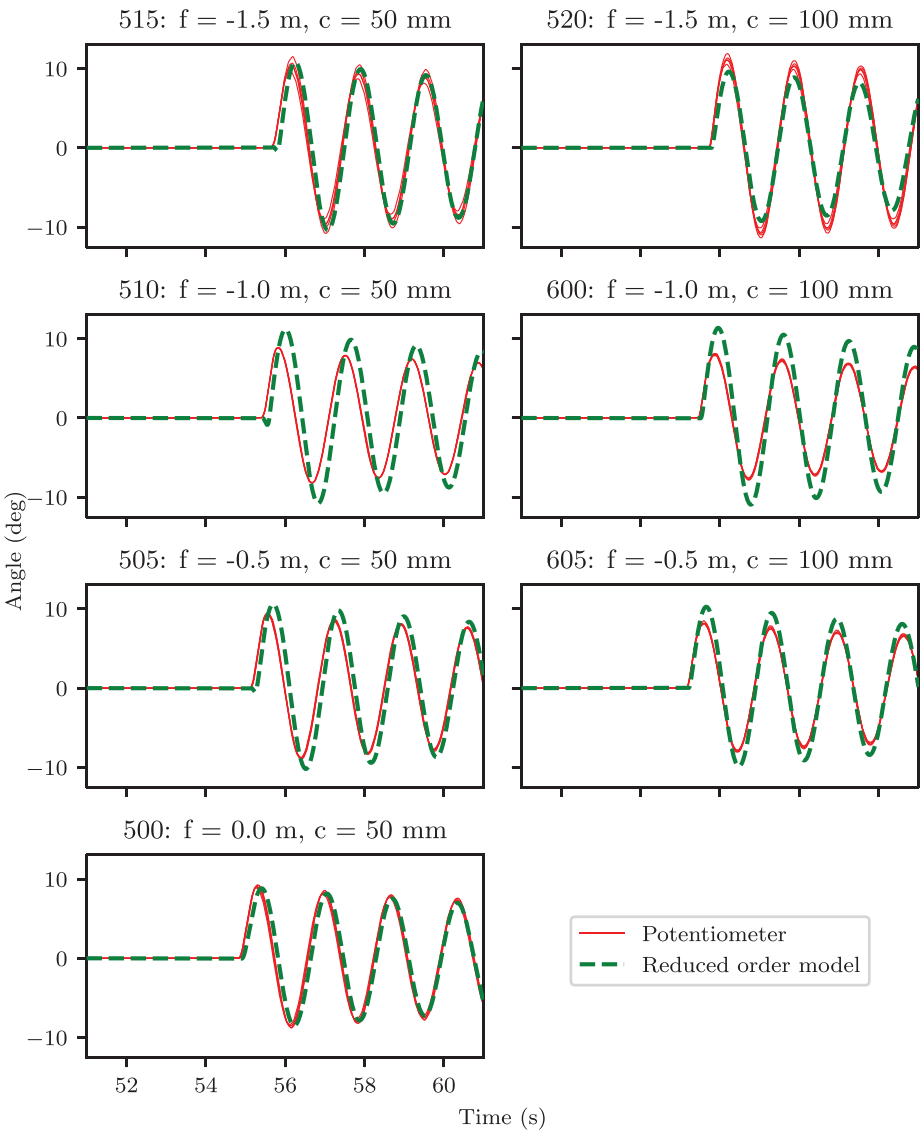

FIG. 10. Pendulum response in a breaking wave as a function of time. Reduced-order model results are compared to the experiment.

CONCLUSIONS

A 2D benchmark experiment for structural deformation in extreme waves was performed by measuring the response of a one degree-of-freedom pendulum with a tube at the base in focused breaking waves. The experiment varied the focus location with respect to the position of the pendulum and the initial vertical clearance between the bottom of the tube and the mean free surface.

The energy in the wave was the same for all tests. The response of the pendulum varied greatly with focus location and initial vertical clearance. It was found that the wave in this data set breaking farthest away, with the pendulum at its highest elevation, caused the largest response. The wave front velocity and the angle of the front were determined by means of image processing of high-speed camera images. Although the largest pendulum response occurs for the largest wave front velocity, and the lowest response for the lowest wave front velocity, the maximum front velocity and angle do not correlate well with the response. The response correlates best with the surface elevation at the position of the pendulum. This was confirmed by the results of a reduced-order model that translates the surface elevation near the pendulum to a force and subsequent response corresponding well with the experimental results, without wave front velocity and angle.

The response also shows variability between experiments in which focus position and initial vertical clearance were kept the same. The variability in surface elevation is caused by the wave components converging over a small distance near the pendulum and the subsequent breaking because the variability in the surface elevation at the first wave gauge is small and the variability in the surface elevation at the position of the pendulum is large. The variability in the response is large when mixing and air entrainment were present. Moreover, the

variability of the pendulum response was always larger than the variability of the surface elevation. The largest variability of the response was observed for the wave breaking farthest away from the position of the pendulum; it is thought that the variability is largest for this condition because here the overturning breaking wave has had the longest time to entrain air and to generate smaller flow structures. The variability in the total response, and hence the impulse, is different from what is observed in literature for breaking waves against rigid, vertical walls for which local pressures in similar wave impacts show variation between tests, but the overall impulse is approximately the same.

ACKNOWLEDGMENTS

We kindly thank the following students for their involvement in this project: Jochem Nonhebel, Bauke Vendeloo, Mike Blom, Sven Klinkhamer, Joris Vleer, Hoang Nguyen, David Pavilons, Bram Hoeksma, and Floris van Ingen. We also thank the technical staff of the towing tank for their support: Jennifer Rodrigues Monteiro, Jasper den Ouden, Pascal Taudin Chabot, Peter Poot, and Frits Sterk.

This work was part of the research programme "SLING" with Project No. P14-10, which is (partly) financed by the Netherlands Organisation for Scientific Research (NWO).

DATA AVAILABILITY

The data that support the findings of this study are openly available in 4TU.ResearchData at http://doi.org/10.4121/13187594, Wellens and Bos (2021).

REFERENCES

Ariyarathne, K., Chang, K., and Mercier, R., "Green water impact pressure on a three-dimensional model structure," Exp. Fluids **53**, 1879 (2012).

Bogaert, H., "An experimental investigation of sloshing impact physics in membrane LNG tanks on floating structures," Ph.D. thesis (Delft University of Technology, 2018).

Bogaert, H., Léonard, S., Marhem, M., Leclère, G., and Kaminski, M., "Hydro-structural behaviour of LNG membrane containment systems under breaking wave impacts: Findings from the Sloshel project," in Proceedings of the 20th International Offshore and Polar Engineering Conference (2010), Vol. 3, pp. 98–108.

Bos, R. W., and Wellens, P. R., "Fluid structure interaction between a pendulum and monochromatic waves," J. Fluids Struct. **100**, 103191 (2021).

Bullock, G. N., Obhrai, C., Peregrine, D. H., and Bredmose, H., "Violent breaking wave impacts. Part 1: Results from large-scale regular wave tests on vertical and sloping walls," Coastal Eng. **54**(8), 602–617 (2007).

Bureau Veritas, "Gas fueled ships for cleaner shipping," http://marine-offshore.bureauveritas.com/insight/gas-fueled-ships-cleaner-shipping, 2018 (last accessed November 19, 2020).

Cheng, Y., and Ji, C., "Numerical simulation of violent breaking wave impacts on a moored offshore wind turbine foundation over nonuniform topography," Phys. Fluids **32**(10), 107106 (2020).

Chuang, W.-L., Chang, K.-A., and Mercier, R., "Impact pressure and void fraction due to plunging breaking wave impact on a 2D TLP structure," Exp. Fluids **58**, 68 (2017).

Cox, D. T., and Ortega, J. A., "Laboratory observations of green water overtopping a fixed deck," Ocean Eng. **29**(14), 1827–1840 (2002).

Faltinsen, O. M., "The effect of hydroelasticity on ship slamming," Philos. Trans. R. Soc. London, Ser. A **355**, 575–591 (1997).

Frihat, M., Karimi, M. R., Brosset, L., and Ghidaglia, J.-M., "Variability of impact pressures induced by sloshing investigated through the concept of 'singularization,'" in Proceedings of the 26th International Offshore and Polar Engineering Conference (2016), Vol. 3, pp. 901–914.

Ghadirian, A., and Bredmose, H., "Pressure impulse theory for a slamming wave on a vertical circular cylinder," J. Fluid Mech. **867**, R1 (2019).

Hofland, B., Kaminski, M. L., and Wolters, G., "Large scale wave impacts on a vertical wall," in Proceedings of the 32nd International Conference on Coastal Engineering (2010).

Ibrahim, R. A., "Assessment of breaking waves and liquid sloshing impact," Nonlinear Dyn. **100**(3), 1837–1925 (2020).

Issa, J. A., Garza-Rios, L. O., Taylor, R. P., Lele, S. P., Rinehart, A. J., Bray, W. H., Tredennick, O. W., Canler, G., and Chapot, K., "Structural capacities of LNG membrane containment systems," in Proceedings of the 19th International Offshore and Polar Engineering Conference (2009), Vol. 3, pp. 107–114.

Lafeber, W., Bogaert, H., and Brosset, L., "Elementary loading processes (ELP) involved in breaking wave impacts: Findings from the Sloshel project," in Proceedings of the International Offshore and Polar Engineering Conference (2012), pp. 265–276.

Lugni, C., Bardazzi, A., Faltinsen, O. M., and Graziani, G., "Hydroelastic slamming response in the evolution of a flip-through event during shallow-liquid sloshing," Phys. Fluids **26**(3), 032108 (2014).

Lugni, C., Brocchini, M., and Faltinsen, O. M., "Wave impact loads: The role of the flip-through," Phys. Fluids **18**(12), 122101 (2006).

Lugni, C., Miozzi, M., Brocchini, M., and Faltinsen, O. M., "Evolution of the air cavity during a depressurized wave impact. I. The kinematic flow field," Phys. Fluids **22**(5), 056101 (2010).

Mai, T., Mai, C., Raby, A., and Greaves, D. M., "Hydroelasticity effects on water-structure impacts," Exp. Fluids **61**(9), 191 (2020).

Mathai, V., Loeffen, L. A. W. M., Chan, T. T. K., and Wildeman, S., "Dynamics of heavy and buoyant underwater pendulums," J. Fluid Mech. **862**, 348–363 (2019).

Morison, J. R., Johnson, J. W., and Schaaf, S. A., "The force exerted by surface waves on piles," J. Pet. Technol. **2**, 149 (1950).

Peregrine, D. H., "Water-wave impact on walls," Annu. Rev. Fluid Mech. **35**, 23–43 (2003).

Sarpkaya, T., "Force on a circular cylinder in viscous oscillatory flow at low Keulegan–Carpenter numbers," J. Fluid Mech. **165**, 61–71 (1986).

van de Bunt, E., Dekker, J., Scharnke, J., and Jaouën, F., "Applying force panels for wave impact measurements," Ocean Eng. **232**, 108857 (2021).

van Meerkerk, M., Poelma, C., Hofland, B., and Westerweel, J., "Experimental investigation of wave tip variability of impacting waves," Phys. Fluids **32**(8), 082110 (2020).

Wang, J., Faltinsen, O. M., and Lugni, C., "Unsteady hydrodynamic forces of solid objects vertically entering the water surface," Phys. Fluids **31**(2), 027101 (2019).

Wellens, P. R., and Bos, R. W. (2021). "Experimental data for a wet-and-dry pendulum in breaking waves," 4TU.ResearchData. https://doi.org/10.4121/13187594